

Local Buckling of Thin-Walled Column of Square Cross-Section Made of In-Plane Coupled Laminate

Andrzej TETER

Damian PASIERBIEWICZ

*Department of Applied Mechanics
Lublin University of Technology
Nadbystrzycka 36 St., PL-20-618 Lublin, Poland*

Zbigniew KOŁAKOWSKI

*Department of Strength of Materials
Lodz University of Technology
Stefanowskiego 1/15, 90-924 Łódź, Poland
Zbigniew.Kolakowski@p.lodz.pl*

Received (15 March 2016)

Revised (25 March 2016)

Accepted (11 April 2016)

The non-symmetric, general laminate exhibits different types of coupling between the extension, shearing, bending and twisting. For practical reasons, the in-plane coupled laminate is a particularly interesting. In this case, the coupling between shearing and extension takes place. Details calculations were performed for a short columns of square cross-section made of in-plane coupled and fully uncoupled laminate under uniform compression. Finite element method (FEM) and analytical-numerical method (ANM) were performed. In FEM analyses, the eigenbuckling problem has been solved using the Lanczos method, whereas the nonlinear buckling analysis were performed using the Newton-Raphson method and the Ritz method. In ANM analyses, the Koiter's asymptotic theory is applied. The relationship between forces/moments and deformations/curvature were described using classical lamination theory (CLT). The coupling between in-plane shearing and extension has a significant influence on the behavior of thin-walled structures under compression.

Keywords: general laminate, buckling, FEM, extension-shearing coupling, CLT, HTCS.

1. Introduction

Layers of a laminate can be arranged in any way. This type of non-symmetric laminates (the so-called: general laminate) exhibits different types of coupling between the extension, shearing, bending and twisting [1-6]. In the literature, the most popular is bending-torsion coupling [7-8]. On the other hand, there are some known arrangement layers for the general laminate, eg. general laminate with 18 plies: [60/-

$60_2/0_3/60_2/0/-60/60_2/-60_3/0_2/60]_T$, where it is possible to fully uncouple the in-plane and out-of-plane response to mechanical and/or thermal loading [9]. For selected laminate stacking sequence, it is possible to observe isolated coupling effects [5–6]. Particularly interesting is the hygro-thermally stable composite laminates (the so-called: HTCS laminates) with coupling which, in the manufacturing process are not warping. In the papers [10–14], the authors have presented a few stacking sequences of the HTCS laminates with different coupling. The current paper focuses on the behavior of compressed thin-walled columns made of general laminate possessing isolated mechanical in-plane coupling, i.e., extension–shearing coupling. There are no other couplings presented. In the literature, a substantial lack of the buckling analysis of thin-walled structures made of coupled laminate is observed. Some effects of mechanical coupling on the post-buckling behavior or vibration analyses of composite laminated structures were studied in the papers [15–19].

2. Characterization of composite laminates

A stacking sequence $[-\theta/\theta]_T$ and a reference system $x-y$ are illustrated in Fig. 1, where a fiber angle is denoted as θ in degree.

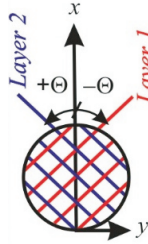


Figure 1 Arrangement of laminate layers

The relationships between forces/moments and deformations/curvatures are described by the stiffness matrix consisting of three submatrices: extensional (**A**), coupling (**B**) and bending (**D**). The constitutive equation can be written in the following form [20–21]:

$$\begin{Bmatrix} \mathbf{N} \\ \mathbf{M} \end{Bmatrix} = \begin{bmatrix} \mathbf{A} & \mathbf{B} \\ \mathbf{B} & \mathbf{D} \end{bmatrix} \begin{Bmatrix} \boldsymbol{\varepsilon} \\ \boldsymbol{\kappa} \end{Bmatrix}, \quad (1)$$

where:

$$\mathbf{A} = \begin{bmatrix} A_{11} & A_{12} & A_{16} \\ & A_{22} & A_{26} \\ Sym. & & A_{66} \end{bmatrix} \quad \mathbf{B} = \begin{bmatrix} B_{11} & B_{12} & B_{16} \\ & B_{22} & B_{26} \\ Sym. & & B_{66} \end{bmatrix} \quad (2)$$

$$\mathbf{D} = \begin{bmatrix} D_{11} & D_{12} & D_{16} \\ & D_{22} & D_{26} \\ Sym. & & D_{66} \end{bmatrix}$$

and $\boldsymbol{\varepsilon}$ – middle surface strain tensor, $\boldsymbol{\kappa}$ – bending and twisting curvatures tensor for the plate element. More details can be found in the Appendix A.

The coupling behavior depends on the form of the elements in each of the submatrices: \mathbf{A} , \mathbf{B} and \mathbf{D} (Eq. 2). The stiffness submatrices for fully uncouple laminate are:

$$\mathbf{A} = \begin{bmatrix} A_{11} & A_{12} & 0 \\ & A_{22} & 0 \\ Sym. & & A_{66} \end{bmatrix} \quad \mathbf{B} = 0 \quad \mathbf{D} = \begin{bmatrix} D_{11} & D_{12} & 0 \\ & D_{22} & 0 \\ Sym. & & D_{66} \end{bmatrix} \quad (3)$$

When the elements: A_{16} and A_{26} are not equal to 0, the coupling between in-plane shear and extension takes place. In this case, the stiffness matrices can be written in the following form:

$$\mathbf{A} = \begin{bmatrix} A_{11} & A_{12} & A_{16} \\ & A_{22} & A_{26} \\ Sym. & & A_{66} \end{bmatrix} \quad \mathbf{B} = 0 \quad \mathbf{D} = \begin{bmatrix} D_{11} & D_{12} & 0 \\ & D_{22} & 0 \\ Sym. & & D_{66} \end{bmatrix} \quad (4)$$

For practical reasons, it is a particularly interesting case of coupling. The in-plane coupled laminates can be produced with modern technology at elevated temperatures. The elements are not warping in the cooling process. An example of the in-plane coupled laminate is laminate with 18 plies [1]: $[45/0/-45/45/-45_5/(0/-45)_3/45_2/-45]_T$.

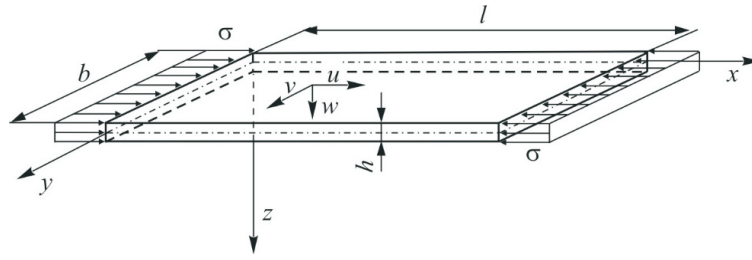


Figure 2 The plate element of the thin-walled structure

3. Analytical–numerical method (ANM)

A plate model has been adopted for the walls of the analyzed laminated column. To describe the middle surface strains the strain tensor for each plate has been assumed in the following form (Fig. 2) [21–26]:

$$\begin{aligned} \varepsilon_x &= u_{,x} + \frac{1}{2}(w_{,x}^2 + v_{,x}^2 + u_{,x}^2) \\ \varepsilon_y &= v_{,y} + \frac{1}{2}(w_{,y}^2 + u_{,y}^2 + v_{,y}^2) \\ 2\varepsilon_{xy} &= \gamma_{xy} = u_{,y} + v_{,x} + w_{,x}w_{,y} + u_{,x}u_{,y} + v_{,x}v_{,y} \end{aligned} \quad (5)$$

where: u, v, w – displacements parallel to the respective axes x, y, z of the local Cartesian system of co-ordinates, whose plane $x - y$ coincides with the middle surface of the plate before its buckling.

Differential equations of equilibrium are [21]:

$$\begin{aligned} N_{x,x} + N_{xy,y} + \{(N_x u_{,x})_{,x} + (N_y u_{,y})_{,y} + (N_{xy} u_{,x})_{,y} + (N_{xy} u_{,y})_{,x}\} &= 0 \\ N_{xy,x} + N_{y,y} + \{(N_x v_{,x})_{,x} + (N_y v_{,y})_{,y} + (N_{xy} v_{,x})_{,y} + (N_{xy} v_{,y})_{,x}\} &= 0 \quad (6) \\ M_{x,xx} + M_{y,yy} + 2M_{xy,xy} + (N_x w_{,x})_{,x} + (N_y w_{,y})_{,y} + (N_{xy} w_{,x})_{,y} \\ + (N_{xy} w_{,y})_{,x} &= 0 \end{aligned}$$

A non-linear stability problem has been solved by using the Koiter's asymptotic theory. The displacement field and sectional force field have been expanded into the power series with respect to the buckling linear eigenvector amplitude (normalized with the equality condition between the maximum deflection and the thickness of the first plate – denote as h). The zero approximation describes the pre-buckling state, whereas the first order approximation allows for determination of critical loads and the buckling modes corresponding to them, taking into account minimisation with respect to the m number of half-waves in the lengthwise direction. The second order approximation is reduced to a linear system of differential heterogeneous equations, whose right-hand sides depend on the force field and the first order displacements only.

Finally, the interaction of N eigenmodes leads to a nonlinear system of equations [21–26]:

$$\left(1 - \frac{\sigma}{\sigma_r}\right) \xi_r + b_{ijr} \xi_i \xi_j + c_{ijk} \xi_i \xi_j \xi_k = \frac{\sigma}{\sigma_r} \xi_r^* \quad r = 1, \dots, N \quad (7)$$

where:

$\zeta_r = w_r/h$ – is the dimensionless amplitude of the r -th buckling mode (w_r – maximum deflection referred to the thickness of the first plate),

$\sigma_r, \zeta_r^* = w_{or}^{\prime}/h$ – are the critical stress and dimensionless amplitude of the initial deflection corresponding to the r -th buckling mode (w_{or} – maximum initial deflection referred to the thickness of the first plate),

N – is the number of interact buckling modes,

b_{ijr} – are the non-linear coefficients in the first order approximations,

c_{ijk} – are the non-linear coefficients in the second approximations.

The range of indexes: i, j, k, r is from 1 to N . The summation is supposed on the repeated indexes. The coefficients b_{ijr} and c_{ijk} can be determined with well-known formulae (see for example [9]). One-mode approach can be written [25]:

$$\left(1 - \frac{\sigma}{\sigma_1}\right) \xi_1 + b_{111} \xi_1^2 + c_{1111} \xi_1^3 = \frac{\sigma}{\sigma_1} \xi_1^*, \quad r = 1 \quad (8)$$

Having found the solutions to the first and the second order boundary problem, the coefficients b_{111}, c_{1111} used to describe postbuckling equilibrium path have been determined [9].

4. Finite Element Method (FEM)

The numerical calculations were performed with the FEM using Abaqus software package (Fig. 3). Discretized model of analysed column was composed of multi-layered shell elements with 8 nodes (type: S8R). The elements have six degree of freedom at each node.

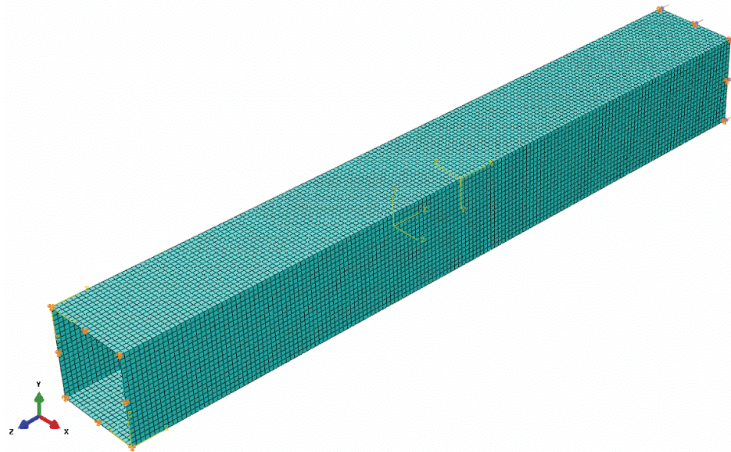


Figure 3 FEM model of the thin-walled structures

The calculations were performed in two stages. At first stage, the eigenbuckling problem have been solved to determine the critical/buckling load with the corresponding buckling mode. In the second stage, the nonlinear buckling analysis was performed to determine the postbuckling behaviour (force vs. displacement relations). The imperfections related to the first buckling mode were implemented to the numerical model with the amplitude of imperfection equal 1/10 of the columns wall thickness. The Newton-Raphson method and the Ritz method (the arc-length method) for solving the nonlinear problem were employed.

5. Comparison of post-buckling paths obtained with FEM and ANM

Detailed calculations were performed for the thin-walled column of square cross-section made of in-plane coupled and fully uncoupled laminate under compression. The former stacking sequence was:

$$[45/0/-45/45/-45_5/(0/-45)_3/45_2/-45/]_T \text{ (denoted as Case 2)}$$

and the latter was the reference one:

$$[60/-60_2/0_3/60_2/0/-60/60_2/-60_3/0_2/60]_T \text{ (denoted as Case 1).}$$

The stiffness submatrices are presented in Tab. 1.

Mechanical properties of the IM7/8552 carbon-epoxy laminate are [1]: Young's moduli moduli in the 1 and 2 material directions: $E_1 = 161$ GPa, $E_2 = 11.38$ GPa, shear modulus in the 1, 2 plane: $G_{12} = 5.17$ GPa, Poisson ratio in the 1, 2 plane: $\nu_{12} = 0.38$. The ply thickness is equal to 0.14 mm.

Table 1 Stiffness submatrices

Case 1 – Laminate without coupling (layup arrangement: [60/ – 60 ₂ /0 ₃ /60 ₂ /0/ – 60/60 ₂ / – 60 ₃ /0 ₂ /60] _T)	Case 2 – Laminate with extension– shearing coupling (layup arrange- ment: [45/0/ – 45/45/ – 45 ₅ /(0/ – 45) ₃ /45 ₂ / –45/] _T)
$\mathbf{A} = \begin{bmatrix} 173846 & 56603 & 0 \\ & 173846 & 0 \\ \text{Sym.} & & 58621 \end{bmatrix}$	$\mathbf{A} = \begin{bmatrix} 190433 & 81757 & -31676 \\ & 105963 & -31676 \\ \text{Sym.} & & 83771 \end{bmatrix}$
$\mathbf{B}=0$	$\mathbf{B}=0$
$\mathbf{D} = \begin{bmatrix} 91999 & 29954 & 0 \\ & 91999 & 0 \\ \text{Sym.} & & 31022 \end{bmatrix}$	$\mathbf{D} = \begin{bmatrix} 92829 & 45514 & 0 \\ & 58485 & 0 \\ \text{Sym.} & & 46575 \end{bmatrix}$

The simulations were conducted for uniformly compressed columns with dimensions of their cross-section shown in Fig. 4.

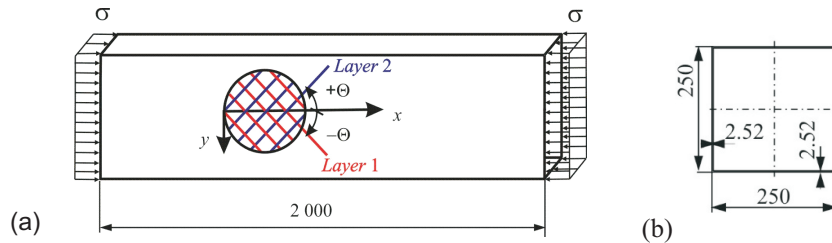


Figure 4 Schematic view of the column and its dimensions in mm

The eigenbuckling problem was solved using the FEM and the ANM methods. Critical stresses for different number of axial half-waves are presented in Tab. 2. All results obtained with both methods were the same. In all cases, the differences were less than 3%. The lowest critical stress was equal to 26 MPa in Case 2 and 23 MPa in Case 1 – Fig. 5. The form corresponding to the lowest flexural buckling load are shown in Fig. 6. It was a local buckling mode with 7 axial half-waves for Case 2 (Fig. 6b) and 8 for Case 1 (Fig. 6a). In this case the increase in the lowest critical stress was 16%.

Table 2 Critical stress versus the number of axial half-waves m (-) for axial compression

$m(-)$	Case 1		Case 2	
	ANM	FEM	ANM	FEM
4	36.0	36.1	33.7	33.2
5	28.5	28.5	29.2	28.7
6	25.0	24.9	27.3	26.9
7	23.5	23.3	26.8	26.1
8	23.1	22.8	27.0	26.3
9	23.4	23.0	27.8	27.3
10	24.3	23.8	29.0	28.4
11	25.5	25.0	30.5	29.9
12	27.1	26.5	32.3	31.7
13	28.9	28.2	34.3	33.7
14	31.1	30.4	36.6	35.9
15	33.4	32.5	39.1	38.4
16	36.0	35.0	41.8	41.0
17	38.8	37.6	44.7	45.2

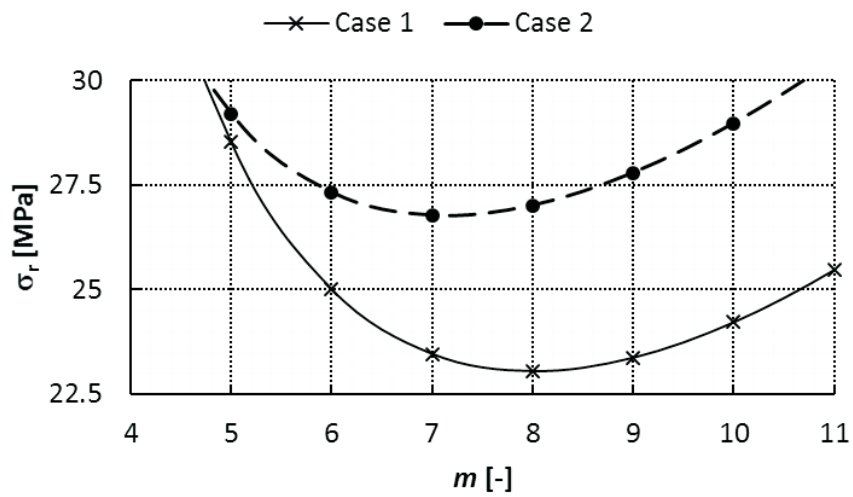


Figure 5 Critical stress versus the number of axial half-waves for axial compression

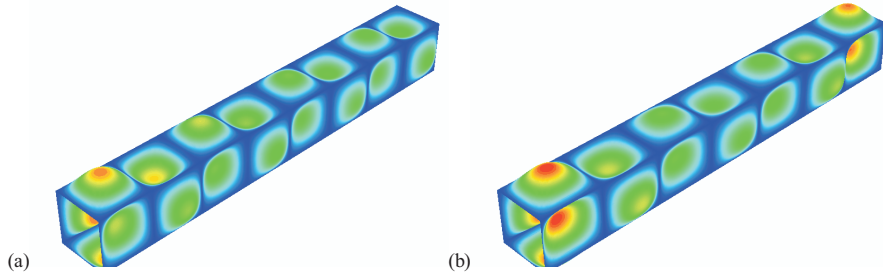


Figure 6 The form corresponding to the lowest flexural buckling load: (a) Case 1 – laminate without coupling, (b) Case 2 – laminate with extension–shearing coupling

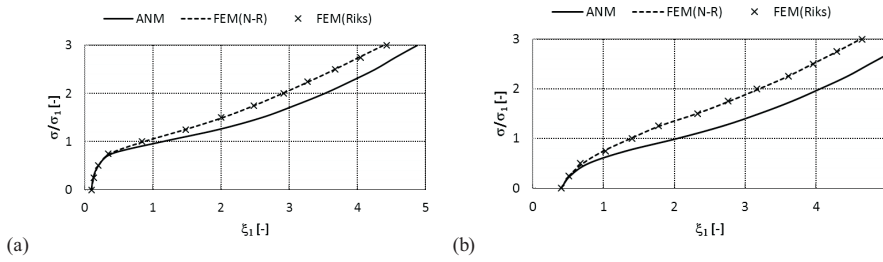


Figure 7 Dimensionless postbuckling paths of the column made of in–plane coupled laminate under compression (Case 2 – $[45/0/-45/45/-455/(0/-45)3/452/-45]/T$), (a) $w_{o1}/h = 0.1$, (b) $w_{o1}/h = 0.4$

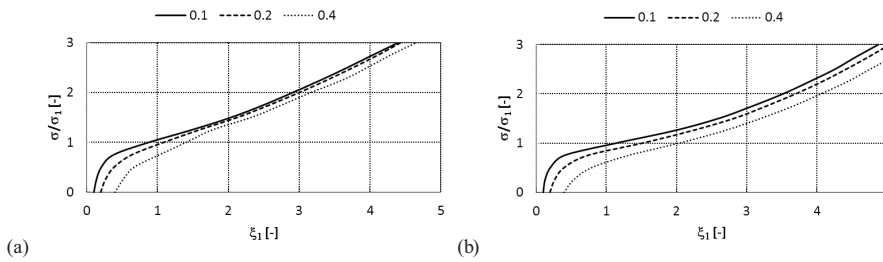


Figure 8 Dimensionless postbuckling paths of the column made of in–plane coupled laminate under compression for different amplitude of initial imperfections (Case 2 – $[45/0/-45/45/-455/(0/-45)3/452/-45]/T$), (a) FEM, (b) A-N

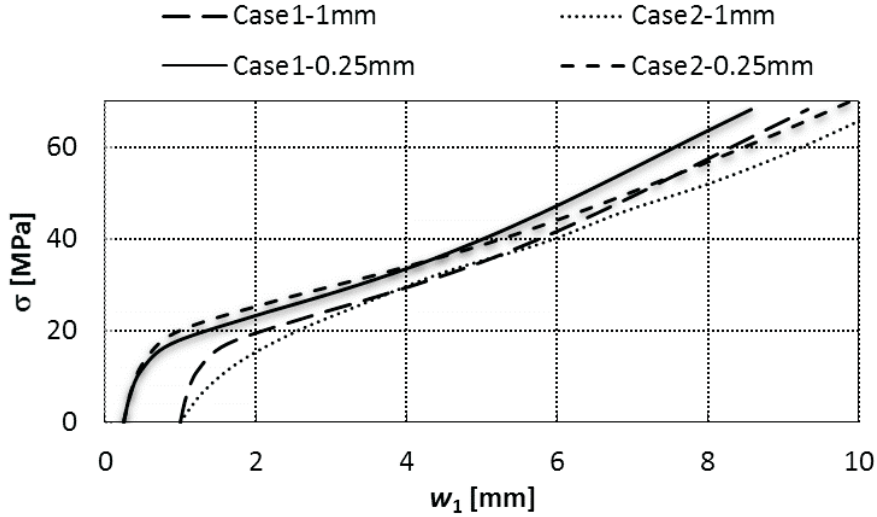


Figure 9 Postbuckling behaviour of the columns made of in-plane coupled (Case 2) and fully uncoupled (Case 1) laminate under compression for different amplitude of initial deflections

The nonlinear problem of buckling was solved using the Newton–Raphson method (denoted as: FEM(N-R)) and the arc-length method (denoted as: FEM(Riks)) in the FEM analysis. The FEM results were compared with the results obtained with the analytical–numerical method (denoted as: ANM). All post–buckling results were shown in Figs. 7–10 for the column made of the in–plane coupled laminate. If the dimensionless loads were low ($\sigma/\sigma_1 < 0.5$ – Fig. 7) and the dimensionless initial deflections were less than 0.4, all the obtained results were identical. On the other hand, if the dimensionless loads were higher, the difference increased significantly but were still at an acceptable level. The ANM results were the lowest ones. The differences yield from the calculation procedure. In the cases of analytical–numerical method (ANM) the one–mode approach was used (see Eq. (7)), while in the case of the FE method the multi–modes approach was accepted.

If the dimensionless loads were higher than 1, the difference between the results obtained by the FEM and the ANM methods was increasing, especially for larger amplitude of initial deflection (compare Fig. 7a and Fig. 7b). In addition, the ANM method was more sensitive to the initial deflection (Fig. 8b) than the FE method (Fig. 8a). If the dimensionless initial deflection changed in the range of 0.1 to 0.4, the postbuckling paths determined by FE method were close to each other (Fig. 8a). In other words, an increase in initial deflection for given loads did not cause an increase in deflections. In that case, the postbuckling paths determined by ANM method strongly dependent on the initial deflection (Fig. 8b). The increase in initial imperfections for the given loads caused a significant increase in deflections.

The use of the in–plane coupled laminates had a significant influence on the post–buckling behavior of the column under compression. Details were shown in Fig. 9. In this case, the post–buckling paths had a lower rigidity in relation to the

columns made of fully uncoupled laminate. This effect was made more visible for large initial deflections. All postbuckling paths were stable and symmetrical.

6. Conclusions

Detailed calculations were performed for the thin-walled column of square cross-section made of in-plane coupled and fully uncoupled laminate. In these cases, the lowest forms of buckling. The designated equilibrium path was stable and symmetrical. For discussed columns high similarity of the computational results were gained. A quantitative and qualitative compatibility was obtained. The coupling between the in-plane shearing and extension had a significant influence on the behavior of thin-walled structures under compression.

Acknowledgements

This paper was financially supported by the Ministerial Research Project No. DEC-2013/11/B/ST8/04358 financed by the Polish National Science Centre.

References

- [1] York, C. B.: On extension–shearing coupled laminates, *Composite Structures*, 120, 472–482, **2015**.
- [2] Shamsudin, M. H. and York, C. B.: Mechanically coupled laminates with balanced plain weave, *Composite Structures*, 107, 416–428, **2014**.
- [3] Valot, E., Vannucci, P. and Verchery, G.: A linear theory for laminates composed of coupled layers, *Composite Structures*, 60, 413–429, **2003**.
- [4] Baker, N., Butler, R. and York, C. B.: Damage tolerance of fully orthotropic laminates in compression, *Composites Science and Technology*, 72, 1083–1089, **2012**.
- [5] York, C. B.: Coupled quasi-homogeneous orthotropic laminates, *Mechanics of Composite Materials*, 47(7), 405–426, **2011**.
- [6] York, C. B.: Characterization of nonsymmetric forms of fully orthotropic laminates, *Journal of Aircraft*, 46(4), 1114–1125, **2009**.
- [7] de Goeij, W. C., van Tooren, M. J. L. and Beukers, A.: Implementation of bending–torsion coupling in the design of a wind–turbine rotor–blade, *Applied Energy*, 63, 191–207, **1999**.
- [8] Murray, R. E., Doman, D. A. and Pegg, M. J.: Finite element modeling and effects of material uncertainties in a composite laminate with bend–twist coupling, *Composite Structures*, 121, 362–376, **2015**.
- [9] Vannucci, P. and Verchery, G.: A special class of uncoupled and quasi-homogeneous laminates, *Composites Science and Technology*, 61, 1465–1473, **2001**.
- [10] Haynes, R. A. and Armanios, E. A.: New families of hygrothermally stable composite laminates with optimal extension–twist coupling, *AIAA Journal*, 48, (12), 2954–2961, **2010**.
- [11] Bhaskar, K., Varadan, T. K. and Ali, J. S. M.: Thermoelastic solutions for orthotropic and anisotropic composite laminates, *Composites, Part B*, 27B, 415–420, **1996**.
- [12] Jin, L. and Daokui, L.: Multi-objective optimization of hygro–thermally curvature–stable antisymmetric laminates with extension–twist coupling, *Journal of Mechanical Science and Technology*, 28, (4), 1373–1380, **2014**.
- [13] Jin, L. and Daokui, L.: Extension–shear coupled laminates with immunity to hygro-thermal shearing distortion, *Composite Structures*, 123, 401–407, **2015**.

- [14] **York, C. B.:** Tapered hygro-thermally curvature-stable laminates with non-standard ply orientations, *Composites, Part A*, 44, 140–148, **2013**.
- [15] **Loughlan, J.:** The influence of mechanical couplings on the compressive stability of anti-symmetric angle-ply laminates, *Composite Structures*, 57, 473–482, **2002**.
- [16] **Ovesy, H. R. and Assaee, H.:** Semi-energy finite strip post-buckling analysis of laminated plates concerning the effects of mechanical coupling, *Composite Structures*, 89, 120–125, **2009**.
- [17] **Walker, M., Adali, S. and Verijenkolg, V.:** Optimization of symmetric laminates for maximum buckling load including the effects of bending-twisting coupling, *Computers & Structures*, 58, (2), 313–319, **1995**.
- [18] **Walker, M., Adali, S. and Verijenkolg, V.:** Optimal design of symmetric angle-ply laminates subject to nonuniform buckling loads and in-plane restraints, *Thin-Walled Structures*, 26, (1), 45–60, **1996**.
- [19] **Band, U. N. and Desai, Y. M.:** Coupled higher order and mixed layerwise finite element based static and free vibration analyses of laminated plates, *Composite Structures*, 128, 406–414, **2015**.
- [20] **Jones, R. M.:** Mechanics of composite materials, *Taylor & Francis, Inc.*, Philadelphia, **1999**.
- [21] **Kořakowski, Z. and Kowal-Michalska, K. (eds.):** Selected problems of instabilities in composite structures, *Wyd. Politechniki Łódzkiej*, **1999**.
- [22] **Teter, A. and Kořakowski, Z.:** Coupled dynamic buckling of thin-walled composite columns with open cross-sections, *Composite Structures*, 95, 28–34, **2013**.
- [23] **Byskov, E. and Hutchinson J. W.:** Mode interaction in axially stiffened cylindrical shells, *AIAA J.*, 15 (7), 941–948, **1977**.
- [24] **van der Heijden, A. M. A. (ed.):** W.T. Koiter's Elastic Stability of Solids and Structures, *Cambridge University Press*, **2009**.
- [25] **Kubiak, T.:** Static and dynamic buckling of thin-walled plate structures, *Springer, Verlag*, London, **2013**.
- [26] **Królak, M. (ed.):** Postbuckling states and load carrying capacity of girders of flat walls, (in Polish), *PWN*, (Polish Scientific Publishers), Warsaw-Lodz, **1990**.

Appendix A.

The stiffness coefficients are defined as [20–21]:

$$A_{ij} = \sum_{k=1}^n (\bar{Q}_{ij})_k (z_k - z_{k-1}) \quad (\text{A1})$$

$$B_{ij} = \frac{1}{2} \sum_{k=1}^n (\bar{Q}_{ij})_k (z_k^2 - z_{k-1}^2) \quad (\text{A2})$$

$$D_{ij} = \frac{1}{3} \sum_{k=1}^n (\bar{Q}_{ij})_k (z_k^3 - z_{k-1}^3) \quad (\text{A3})$$

where: z_k represent the height relative to the laminate mid-plane for the k -th ply.

The transformed reduced stiffness terms \bar{Q}_{ij} are given by [20-21]:

$$\bar{Q}_{11} = Q_{11} \cos^4 \theta + 2(Q_{12} + 2Q_{66}) \cos^2 \theta \sin^2 \theta + Q_{22} \sin^4 \theta \quad (\text{A4})$$

$$\bar{Q}_{12} = \bar{Q}_{21} = (Q_{11} + Q_{22} - 4Q_{66}) \cos^2 \theta \sin^2 \theta + Q_{12} (\cos^4 \theta + \sin^4 \theta) \quad (\text{A5})$$

$$\bar{Q}_{16} = \bar{Q}_{61} = [(Q_{11} - Q_{12} - 2Q_{66}) \cos^2 \theta + (Q_{12} - Q_{22} + 2Q_{66}) \sin^2 \theta] \cos \theta \sin \theta \quad (\text{A6})$$

$$\bar{Q}_{22} = Q_{11} \sin^4 \theta + 2(Q_{12} + 2Q_{66}) \cos^2 \theta \sin^2 \theta + Q_{22} \cos^4 \theta, \quad (\text{A7})$$

$$\bar{Q}_{26} = \bar{Q}_{62} = [(Q_{11} - Q_{12} - 2Q_{66}) \sin^2 \theta + (Q_{12} - Q_{22} + 2Q_{66}) \cos^2 \theta] \cos \theta \sin \theta \quad (\text{A8})$$

$$\bar{Q}_{66} = (Q_{11} + Q_{22} - 2Q_{12} - 2Q_{66}) \cos^2 \theta \sin^2 \theta + Q_{66} (\cos^4 \theta - \sin^4 \theta) \quad (\text{A9})$$

where:

$$Q_{11} = \frac{E_1}{1-\nu_{12}\nu_{21}}, \quad Q_{12} = \frac{\nu_{12}E_2}{1-\nu_{12}\nu_{21}} = \frac{\nu_{21}E_1}{1-\nu_{12}\nu_{21}}, \quad (\text{A10})$$

$$Q_{11} = \frac{E_2}{1-\nu_{12}\nu_{21}}, \quad Q_{66} = G_{12}$$

and mechanical properties are denoted as: Young's moduli in the 1 and 2 material directions: E_1, E_2 , shear modulus in the 1, 2 plane: G_{12} , Poisson ratio in the 1, 2 plane: ν_{12} .

To determine the resultant moments \mathbf{M} and forces \mathbf{N} acting on the laminate, the k -th ply stresses are integrated through the ply thickness and the sum of the effects from all the plies is then taken in the following manner [21]:

$$\begin{Bmatrix} M_x \\ M_y \\ M_{xy} \end{Bmatrix} = \sum_{k=1}^p \int_{z_{k-1}}^{z_k} \begin{Bmatrix} \sigma_x \\ \sigma_y \\ \tau_{xy} \end{Bmatrix}_k dz \quad (\text{A11})$$

$$\begin{Bmatrix} N_x \\ N_y \\ N_{xy} \end{Bmatrix} = \sum_{k=1}^p \int_{z_{k-1}}^{z_k} \begin{Bmatrix} \sigma_x \\ \sigma_y \\ \tau_{xy} \end{Bmatrix}_k dz$$

and

$$\begin{Bmatrix} M_x \\ M_y \\ M_{xy} \end{Bmatrix} = \sum_{k=1}^p \begin{bmatrix} \bar{Q}_{11} & \bar{Q}_{12} & \bar{Q}_{16} \\ \bar{Q}_{21} & \bar{Q}_{22} & \bar{Q}_{26} \\ \bar{Q}_{61} & \bar{Q}_{62} & \bar{Q}_{66} \end{bmatrix}_k \left[\int_{z_{k-1}}^{z_k} \begin{Bmatrix} \varepsilon_x \\ \varepsilon_y \\ \gamma_{xy} \end{Bmatrix}_k z dz + \int_{z_{k-1}}^{z_k} \begin{Bmatrix} \kappa_x \\ \kappa_y \\ 2\kappa_{xy} \end{Bmatrix}_k z^2 dz \right]$$

$$\begin{Bmatrix} N_x \\ N_y \\ N_{xy} \end{Bmatrix} = \quad (A12)$$

$$\sum_{k=1}^p \begin{bmatrix} \bar{Q}_{11} & \bar{Q}_{12} & \bar{Q}_{16} \\ \bar{Q}_{21} & \bar{Q}_{22} & \bar{Q}_{26} \\ \bar{Q}_{61} & \bar{Q}_{62} & \bar{Q}_{66} \end{bmatrix}_k \left[\int_{z_{k-1}}^{z_k} \begin{Bmatrix} \varepsilon_x \\ \varepsilon_y \\ \gamma_{xy} \end{Bmatrix}_k dz + \int_{z_{k-1}}^{z_k} \begin{Bmatrix} \kappa_x \\ \kappa_y \\ 2\kappa_{xy} \end{Bmatrix}_k z dz \right]$$

$$\begin{Bmatrix} M_x \\ M_y \\ M_{xy} \end{Bmatrix} =$$

$$\begin{bmatrix} B_{11} & B_{12} & B_{16} \\ B_{21} & B_{22} & B_{26} \\ B_{61} & B_{62} & B_{66} \end{bmatrix} \begin{Bmatrix} \varepsilon_x \\ \varepsilon_y \\ \gamma_{xy} \end{Bmatrix} + \begin{bmatrix} D_{11} & D_{12} & D_{16} \\ D_{21} & D_{22} & D_{26} \\ D_{61} & D_{62} & D_{66} \end{bmatrix} \begin{Bmatrix} \kappa_x \\ \kappa_y \\ \kappa_{xy} \end{Bmatrix},$$

$$\begin{Bmatrix} N_x \\ N_y \\ N_{xy} \end{Bmatrix} = \quad (A13)$$

$$\begin{bmatrix} A_{11} & A_{12} & A_{16} \\ A_{21} & A_{22} & A_{26} \\ A_{61} & A_{62} & A_{66} \end{bmatrix} \begin{Bmatrix} \varepsilon_x \\ \varepsilon_y \\ \gamma_{xy} \end{Bmatrix} + \begin{bmatrix} B_{11} & B_{12} & B_{16} \\ B_{21} & B_{22} & B_{26} \\ B_{61} & B_{62} & B_{66} \end{bmatrix} \begin{Bmatrix} \kappa_x \\ \kappa_y \\ \kappa_{xy} \end{Bmatrix}$$

